Ordered Mesoporous Microspheres for Bone Grafting and Drug Delivery

D. Arcos,[†,‡] A. López-Noriega,[†,‡] E. Ruiz-Hernández,[†,‡] O. Terasaki,[§] and M. Vallet-Regí*[,†,‡]

Departamento de Química Inorgánica y Bioinorgánica, Facultad de Farmacia, Universidad Complutense de Madrid, Madrid, Spain, Networking Research Center on Bioengineering, Biomaterials and Nanomedicine (CIBER-BBN), Madrid, Spain, and Structural Chemistry, Arrhenius Laboratory, Stockholm University, S-10691 Stockholm, Sweden

Received June 17, 2008. Revised Manuscript Received January 16, 2009

Bioactive microspheres with ordered mesoporous structure have been synthesized by means of the evaporation-induced self-assembly (EISA) method and following an aerosol-assisted route. The bioactive microspheres belong to the $SiO_2-CaO-P_2O_5$ systems, and the mesoporous structure closely depends on the structure-directing agent as well as its interaction with the Ca^{2+} cations during the mesophase formation. Among the different tested surfactants, the triblock copolymer F127 leads to hexagonal ordered structures for low CaO contents, P123 leads to wormlike mesoporous structures for any CaO content, whereas the ionic surfactant cetyltrimethyl ammonium bromide (C_{16}TAB) does not produce accessible mesopores at the external surface, for any CaO content. All the mesoporous $SiO_2-CaO-P_2O_5$ microspheres develop an apatite like layer when reacting with simulated body fluid. Preliminary tests indicate the capability to load and release triclosan with kinetic profiles that depend on the pore structure, thus showing interesting features to be used in periodontal regenerative surgery and infection profilaxis.

Introduction

In recent years, research on mesoporous materials with potential applications in the field of biomedicine has significantly increased. Because these materials demonstrated the capability to load and release large amounts of drugs,[1] an important evolution has been carried out on the basis of their promising characteristics as drug delivery systems.[2] In this sense, different chemical surface functionalizations for a more efficient charge and delivery of drugs,[3] proteins,[4] and even DNA[5] have been studied. Moreover, stimuli responsive[6] or drug magnetic targeting systems[7] have been developed from mesoporous materials. Composites of silica nanoparticles associated with biopolymers have shown properties as potential drug delivery applications.[8−10] In addition, the fabrication of silica-based nanocapsules has opened new perspectives to the technology of biomolecules immobilization[11] or even bacteria encapsulation.[12]

In addition to their outstanding textural parameters,[13,14] which provide them the ability to act as drug carriers, silica-based mesoporous materials have also shown a slightly bioactive behavior.[15] This attribute opened the possibility to use these materials for bone tissue regeneration and dental reconstruction. However, bioactive kinetics shown by conventional mesoporous materials such as SBA-15, MCM-41, or MCM-48 is too slow to be acceptable from a clinical point of view. In this sense, advances have been produced as well, leading to the obtaining of highly bioactive mesoporous materials in the system $SiO_2-CaO-P_2O_5$.[16−21] These bioactive templated glasses have been conformed as macro−mesoporous materials for scaffolds in tissue engineering[22−25] and the first drug delivery tests have been carried with them,[26] showing very promising results.

Most of the synthetic methods to achieve SiO_2-based mesoporous materials lead to the obtaining of irregularly

* Corresponding author. Phone: 34 91 3941870. Fax: 34 91 3941786. E-mail: vallet@farm.ucm.es.
† Universidad Complutense de Madrid.
‡ Networking Research Center on Bioengineering, Biomaterials and Nanomedicine.
§ Stockholm University.

(1) Vallet-Regí, M.; Rámila, A.; Del Real, R. P.; Pérez-Pariente, J. *Chem. Mater.* **2001**, *13*, 308.
(2) (a) Vallet-Regí, M.; Balas, F.; Arcos, D. *Angew. Chem., Int. Ed.* **2007**, *46*, 7548. (b) Vallet-Regí, M.; Balas, F.; Colilla, M.; Manzano, M. *Prog. Solid State Chem.* **2008**, *36*, 163.
(3) Balas, F.; Manzano, M.; Horcajada, P.; Vallet-Regí, M. *J. Am. Chem. Soc.* **2006**, *128*, 8116.
(4) Slowing, I. I.; Trewyn, B. G.; Lin, V. S.-Y. *J. Am. Chem. Soc.* **2007**, *129*, 8845.
(5) Torney, F.; Trewyn, B. G.; Lin, V. S.-Y.; Wang, K. *Nature Nanotech.* **2007**, *2*, 295.
(6) Giri, S.; Trewyn, B. G.; Stellmaker, M. P.; Lin, V. S.-Y. *Angew. Chem., Int. Ed.* **2005**, *44*, 5038.
(7) Ruiz-Hernández, E.; López-Noriega, A.; Arcos, D.; Izquierdo-Barba, I.; Terasaki, O.; Vallet-Regí, M. *Chem. Mater.* **2007**, *19*, 3455.
(8) Coradin, T.; Livage, J. *Acc. Chem. Res.* **2007**, *40*, 819.
(9) Allouche, J.; Boissiere, M.; Helary, C.; Livage, J.; Coradin, T. *J. Mater. Chem.* **2006**, *16*, 3120.
(10) Boissiere, M.; Meaows, P. J.; Brayner, R.; Helary, C.; Livage, J.; Coradin, T. *J. Mater. Chem.* **2006**, *16*, 1178.
(11) Avnir, D.; Coradin, T.; Lev, O.; Livage, J. *J. Mater. Chem.* **2006**, *16*, 1013.
(12) Nassif, N.; Roux, C.; Coradin, T.; Pager, M. N.; Bouvet, O. M. M.; Livage, J. *J. Mater. Chem.* **2003**, *13*, 203.
(13) Kresge, C. T.; Leonowicz, M. E.; Roth, W. J.; Vartuli, J. C.; Beck, J. S. *Nature* **1992**, *359*, 710.
(14) Beck, J. S.; Vartuli, J. C.; Roth, W. J.; Leonowicz, M. E.; Kresge, C. T.; Schmitt, K. D.; Chu, C. T. W.; Olson, D. H.; Sheppard, E. W.; McCullen, S. B.; Higgins, J. B.; Schlenker, J. L. *J. Am. Chem. Soc.* **1992**, *114*, 10834.
(15) Izquierdo-Barba, I.; Ruiz-González, L.; Doadrio, J. C.; González, J. M.; Vallet-Regí, M. *Solid State Sci.* **2005**, *7*, 983.

10.1021/cm801649z CCC: $40.75
Published on Web 02/13/2009

shaped particles. The use of an aerosol-assisted synthesis allows producing mesoporous materials in the form of spheres of a micrometric size.[7,27−29] Control over both the external morphology and the mesostructure of the material leads to the development of more reliable and reproducible drug delivery systems.[30,31] Moreover, enforcing bioactive behavior on such microspheric materials would result in a potential use as hard tissue repair systems. To date, few experiments have considered the obtaining of mesoporous bioactive materials in the form of microspheres,[32] which are widely accepted from a clinical point of view because they can be injected or dispersed into bone cements as they are able to form stable suspensions.[23−36]

In the present work, the synthesis of bioactive mesoporous microspheres in the system $SiO_2-CaO-P_2O_5$ showing an ordered mesopore arrangement is reported for the first time. The effect of the addition of CaO over the structural and textural parameters of different ordered spherical mesoporous materials is evaluated. Bioactivity of different mesoporous microspheres is also studied. Finally, drug loading and releasing from bioactive microspheres is evaluated using triclosan, which is a widely used antimicrobial agent[37,38] in the treatment of supragingival plaque. These materials thus present potential applications in periodontal regenerative surgery and infection profilaxis.

Experimental Section

Three series of different bioactive mesoporous microspheres (BMS) were synthesized following an evaporation induced self-assembly (EISA) method, assisted by an aerosol route and using three different structure directing agents: one cationic (Hexadecyltrimethyl-ammonium bromide-CTAB) and two nonionic amphiphilic triblock copolymers with different hydrophilic chains length (Pluronic P123 [(ethylene oxide, $EO)_{20}$(propylene oxide, $PO)_{70}(EO)_{20}$] and Pluronic F127 [$(EO)_{106}(PO)_{70}(EO)_{106}$]). To study the influence of the inclusion of CaO in the mesoporous network over the characteristics of the materials, microspheres with 100% SiO_2 and different $SiO_2-CaO-P_2O_5$ molar composition were synthesized. Constant 5% molar content of P_2O_5 was included to accelerate the in vitro bioactive process of these microspheres, i.e., decreasing the nucleation time and growth of an apatite-like phase on the microsphere surface, when soaked into simulated body fluid (SBF). Samples were denoted BMS100*x*, BMS85*x*, BMS75*x* and BMS58*x* as a function of SiO_2 content (% mol) being *x*= C, P, or F for samples synthesized with CTAB, P123, and F127, respectively. For comparison purposes, microspheres without surfactant were also synthesized and coded BMS100* and BMS85*. Table S1 (see the Supporting Information) shows all the compositions of the BMSs synthesized in this work.

Tetraethoxysilane ($[Si(OCH_2CH_3)_4]$, TEOS), triethyl phosphate ($[PO_4(CH_2CH_3)_3]$, TEP), and calcium nitrate ($Ca(NO_3)_2.4H_2O$) were used as precursors of SiO_2, P_2O_5, and CaO, respectively. Triclosan (5-chloro-2-(2,4-dichloro-phenoxy)phenol) and CTAB were purchased from Sigma-Aldrich and used without further purification. Pluronic P123 and F127 were obtained as a gift from BASF.

Preparation of the Precursor Solution. In a typical preparation, for a BMS85*x* composition 7.61 g of the corresponding structure directing agent (25% weight respecting to TEOS) were dissolved in a solution of 670 mL of ethanol, 5.6 mL of HNO_3 6 M and 38.08 mL of water. After 3 h of stirring, 29.58 mL of TEOS, 2.62 mL of TEP and 3.58 g of calcium nitrate were added consecutively to the solution in three hours intervals. Afterward, the solution was kept stirring overnight. Same synthesis procedure was used for pure silica mesoporous microspheres but adding only the SiO_2 precursor.

Fabrication of the Bioactive Microspheres. BMS were synthesized by pyrolisis of an aerosol generated by ultra high frequency spraying of the precursor solution, following a technique addressed before.[7,39−41] Briefly, this process is based on the use of a piezoelectric ceramic, which is placed below the precursor solution of the material. When the piezoelectric transducer is excited near its own resonance frequency (about 850 kHz for the transducer used), a geyser is formed at the surface of the liquid. This geyser produces ultrafine droplets, which form an aerosol. N_2 gas is used as the carrier to convey the aerosol to the preheating zone, where the solvent evaporation occurs triggering the micellar self-assembly. Thereafter, the droplets go through the pyrolisis zone, which consists of a 65 cm long tubular furnace at 400 °C. The residence time of the particles in the high-temperature zone (in our case, 2 s) is controlled by the gas flow, which was fixed to 8 L min^{-1}. Particles are collected outside the furnace with an electrostatic filter, consisting in a thin tungsten wire suspended in the center of a tubular stainless steel collection plate. This wire is negatively charged with 8 kV and thus the particles become charged and are collected on the plate. All the transport zone of the aerosol is kept at 100 °C so that ethanol condensation is avoided.

(16) Yan, X. X.; Yu, C. Z.; Zhou, X. F.; Tang, J. W.; Zhao, D. Y. *Angew. Chem., Int. Ed.* **2004**, *43*, 5980.
(17) Izquierdo-Barba, I.; Arcos, D.; Sakamoto, Y.; Terasaki, O.; López-Noriega, A.; Vallet-Regí, M. *Chem. Mater.* **2008**, *20*, 3191.
(18) Yan, X. X.; Huang, X. H.; Yu, C. Z.; Deng, H. X.; Wang, Y.; Zhang, Z. D.; Qiao, S. Z.; Lu, G. Q.; Zhao, D. Y. *Biomaterials* **2006**, *27*, 3396.
(19) Shi, Q. H.; Wang, J. F.; Zhang, J. P.; Fan, J.; Stucky, G. D. *Adv. Mater.* **2006**, *18*, 1038.
(20) López-Noriega, A.; Arcos, D.; Izquierdo-Barba, I.; Sakamoto, Y.; Terasaki, O.; Vallet-Regí, M. *Chem. Mater.* **2006**, *18*, 3137.
(21) Yun, H. S.; Kim, S. E.; Hyeon, Y. T. *Mater. Lett.* **2007**, *61*, 4569.
(22) Yun, H. S.; Kim, S. E.; Hyeon, Y. T. *Chem. Commun.* **2007**, *21*, 2139.
(23) Yun, H. S.; Kim, S. E.; Hyun, Y. T.; Heo, S. J.; Shin, J. W. *Chem. Mater.* **2007**, *19*, 6363.
(24) Li, X.; Wang, X. P.; Chen, H. R.; Jiang, P.; Dong, X. P.; Shi, J. L. *Chem. Mater.* **2007**, *19*, 4322.
(25) Yi, J.; Wei, G. F.; Huang, X. H.; Zhao, L. Z.; Zhang, Q.; Yu, C. Z. *J. Sol−Gel Sci. Technol.* **2008**, *45*, 115.
(26) Xia, W.; Chang, J. *J. Controlled Release* **2006**, *110*, 522.
(27) Lu, Y.; Fan, H.; Stump, A.; Ward, T. L.; Rieker, T.; Brinker, C. J. *Nature* **1999**, *398*, 223.
(28) Rama Rao, G. V.; López, G. P.; Bravo, J.; Pham, H.; Datye, A. K.; Xu, H.; Ward, T. L. *Adv. Mater.* **2002**, *14*, 1301.
(29) Julián-López, B.; Boissiere, C.; Chaneac, C.; Grosso, D.; Vasseur, S.; Miraux, S.; Duguet, E.; Sánchez, C. *J. Mater. Chem.* **2007**, *17*, 1563.
(30) Qu, F. Y.; Zhu, G. S.; Huang, S. Y.; Li, S. G.; Sun, J. Y.; Zhang, D. L.; Qiu, S. L. *Microporous Mesoporous Mater.* **2006**, *92*, 1.
(31) Li, X.; Zhang, L. X.; Dong, X. P.; Liang, J.; Shi, J. L. *Microporous Mesoporous Mater.* **2007**, *102*, 151.
(32) Ostomel, T. A.; Shi, Q. H.; Tsung, C. K.; Liang, H. J.; Stucky, G. D. *Small* **2006**, *2*, 1261.
(33) Vasir, J. K.; Tambwekar, K.; Garg, S. *Int. J. Pharm.* **2003**, *255*, 13.
(34) Edlund, U.; Albertsson, A. C. *Adv. Polym. Sci.* **2002**, *157*, 67.
(35) Kawaguchi, H. *Prog. Polym. Sci.* **2000**, *25*, 1171.
(36) Freiberg, S.; Zhu, X. X. *Int. J. Pharm.* **2004**, *282*, 1.
(37) Kockisch, S.; Rees, G. D.; Tsibouklis, J.; Smart, J. D. *Eur. J. Pharm. Biopharm.* **2005**, *59*, 207.
(38) Pei, A. H.; Shen, Z. W.; Yang, G. S. *Mater. Lett.* **2007**, *61*, 2757.
(39) Vallet-Regí M. Preparative strategies for controlling structure and morphology of metal oxides. In *Perspectives in Solid State Chemistry*; Rao, K. J., Ed.; Narosa: New Delhi, India, 1995; Vol. 37
(40) Cabañas, M. V.; Vallet-Regí, M.; Labeau, M. *J. Mater. Res.* **1993**, *8*, 2694.
(41) Martínez, A.; Peña, J.; Labeau, M.; González-Calbet, J. M.; Vallet-Regí, M. *J. Mater. Res.* **1995**, *10*, 1307.

To remove both the surfactant and the nitrate groups from the product, we calcined the powder obtained by the aerosol-assisted method in air at 700 °C for 3 h.

Assessment of In vitro Bioactivity. Assessment of in vitro bioactivity was carried out both on powder and on disk-shaped samples. Disks were fabricated by softly pressing 50 mg of the powder under 1 ton during 1 min in order to keep the mesoporous structure. Disks were soaked in 10 mL of filtered simulated body fluid (SBF) in polyethylene containers at 37 °C under sterile conditions. SBF has similar composition and ionic concentrations to those of human plasma.[42] The evolution of the surface of the materials was studied by scanning electron microscopy (SEM) and Fourier transform infrared (FTIR) spectroscopy using attenuated total reflection (ATR).

The ions release rate from the materials to the surrounding media was followed as a function of soaking time. Ca, Si, and P concentration of the SBF were determined by inductively coupled plasma spectroscopy (ICP).

In vitro Drug Release Assay. To study the influence of the mesostructure on the drug release, the tests were carried out only with those $SiO_2-CaO-P_2O_5$ microspheres that, having the same chemical composition, exhibited clear differences in the degree of mesopore ordering (see below). Therefore, 1 g of BMS85F, BMS85P, and BMS85C were added into 100 mL of a solution of triclosan in ethanol (20 mg mL^{-1}), where it was stirred strongly for 48 h at room temperature while the evaporation of ethanol was prevented. Loaded materials were then filtered under a vacuum and washed with 10 mL of ethanol. This process was repeated 4 times with each sample. After the loaded BMSs were dried at 37 °C for 24 h, 100 mg of each one was immersed into 10 mL of filtered 2 M tris-buffer solution with pH 7.4 at 37 °C under stirring at 100 rpm. Samples of 1 mL were removed at given time intervals, diluted to 10 mL with tris-buffer, and analyzed by UV−visible spectroscopy at a wavelength of 282 nm. The volume removed was replaced with the same amount of preheated filtered tris-buffer. The experiments were carried out in triplicate.

The determinations of the triclosan loading in the materials were carried out by thermogravimetric (TG) analyses using a Seiko Thermobalance TG/DTA 320, as well as CHN elemental microanalyses.

Characterization. Powder X-ray diffraction (XRD) experiments were performed with a Philips X'Pert diffractometer equipped with Cu Kα radiation (wavelength 1.5406 Å). XRD patterns were collected in the 2θ ranges between 0.6 and 6°, and from 10 to 60° with a step size of 0.02° and counting time of 5 and 10 s per step, respectively.

The textural properties of the materials were determined by nitrogen sorption porosimetry by using a Micromeritics ASAP 2010. To perform the N_2 measurements, the samples were previously degassed under a vacuum for 24 h at 120 °C. The surface area was determined using the Brunauer−Emmett−Teller (BET) method. The pore size distribution between 0.5 and 40 nm was determined from the desorption branch of the isotherm by means of the Barret−Joyner−Halenda (BJH) method.

Transmission electron microscopy (TEM) was carried out with a JEOL JEM 2000 FX instrument operated at 200 kV equipped with a LINK AN 10000 analytical system and CCD camera (KeenView Camera). Fourier patterns were conducted using CRISP program. Sample preparation was carried out by crushing and dispersing in ethanol. Finally, they were deposited onto carbon-coated copper grids.

Scanning electron microscopy (SEM) analyses were made on a JEOL 6400-LINK AN 10 000 microscope (Electron Microscopy Centre, UCM). The samples were prepared by placing them onto a graphite sticky tape over the holder and a posterior Au metallization. FTIR analyses were carried out in a Nicolet Magma IR 550 spectrometer. UV−visible spectroscopy was performed in a UNICAM UV 500 spectrometer between 200 and 500 nm. Dynamic Light Scattering (DLS) measurements were obtained on a Zetasizer Nano ZS (Malvern Instruments) equipped with a 633 nm "red" laser to determinate BMS size.

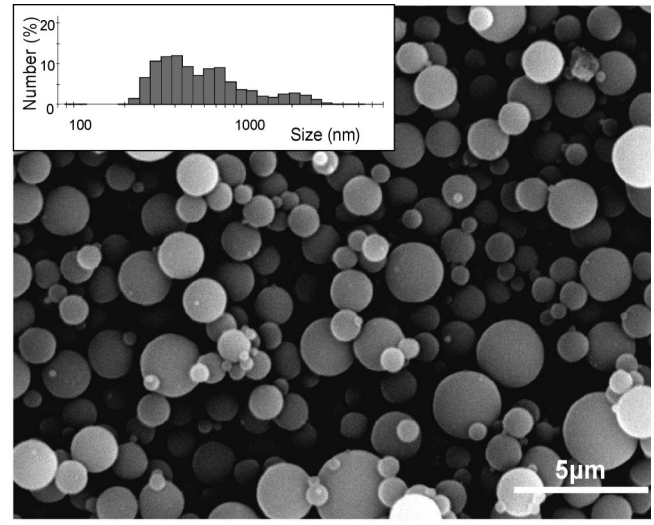

Figure 1. SEM micrograph of BMS85P. Magnification 5000×. Inset shows particle size distribution determined by DLS measurements.

Results

Figure 1 shows as an example a representative SEM micrograph obtained from BMS85P. The surface of the microspheres is smooth and no aggregation among them is observed. The inset shows particle size distribution obtained from DLS measurements. These spheres are heterogeneous in size, with a diameter distribution from 0.2 to 3 μm, centered on 400 nm. Pure SiO_2 microspheres and those synthesized with different structure-directing agents following this synthetic procedure show neither morphological nor size distribution differences to those shown in Figure 1.

Small-angle XRD patterns of the spheres synthesized with different surfactants and compositions are collected in Figure 2. This figure only shows those XRD patterns that exhibit some X-ray scattering along the small angle interval (Figures S1 and S2 in the Supporting Information show the patterns for compositions with higher CaO content). Pure silica material synthesized with CTAB as structure-directing agent (BMS100C) shows a unique maximum at $2\theta = 2.9°$, corresponding to a d spacing of 2.8 nm. This maximum can be assigned to the 1 0 reflection of a 2d hexagonal ($p6m$) structure, according to TEM observations and previous results.[27] This maximum becomes broader and significantly weaker with the addition of 10% CaO and 5% P_2O_5 to the mesoporous network (BMS85C), suggesting a defective arrangement of the mesopores. This fact was further confirmed by TEM observations. The same is observed in microspheres prepared with P123. In this case, the only maximum observed ($2\theta = 0.96°$, d spacing of 9.4 nm) can be assigned to the 1 0 reflection of a hexagonal phase[16] and also change to a broad and weak maximum when 10 mol %

(42) Kokubo, T.; Kushitani, H.; Sakka, S.; Kitsugi, T.; Yamamuro, T. *J. Biomed. Mater. Res.* **1990**, *24*, 721.

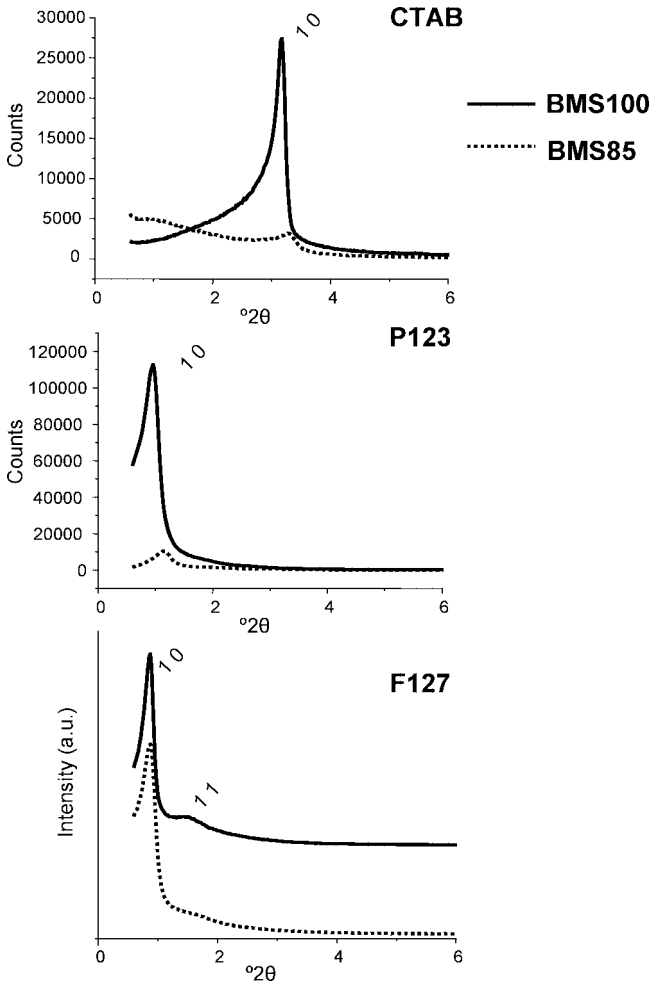

Figure 2. Small-angle X-ray diffraction patterns of BMS100x and BMS85x microspheres synthesized with CTAB, P123, and F127 as structure-directing agents. BMS75x and BMS58x microspheres do not show diffraction maxima, and their patterns are available asSupporting Information.

CaO and 5 mol % P_2O_5 are added to the synthesis (BMS85P). Samples with higher content of Ca^{2+} (such as BMS75P and BMS58P with 20 and 37 mol %, respectively), do not exhibit any order (see the Supporting Information), indicating the important and negative influence of Ca^{2+} cations on the mesophase formation during the inorganic−micelle composite self-assembly. In the case of mesoporous materials synthesized with F127, BMS100F and BMS85F compositions show almost identical diffraction patterns. Two diffraction maxima can be distinguished at $2\theta = 0.87$ and 1.5°, with *d* spacing of 9.8 and 5.2 nm, respectively. TEM observations (see below) allowed us to assign them to reflections 1 0 and 1 1 of a 2d hexagonal phase *p6m*. Higher CaO amounts like in BMS75F lead to microspheres with very defective ordered structure, whereas BMS58F exhibits a XRD pattern corresponding to a completely disordered sample (see the Supporting Information).

From the scattering degree observed in XRD patterns, only those microspheres of BMS100x and BMS85x compositions indicated the possibility of some mesopore ordering. Therefore, TEM studies were carried out on those samples. Figure 3 shows the TEM images of pure silica microspheres (BMS100x) and 85 SiO_2-10 CaO-5 P_2O_5 compositions (BMS85x) for the three different surfactants used in this

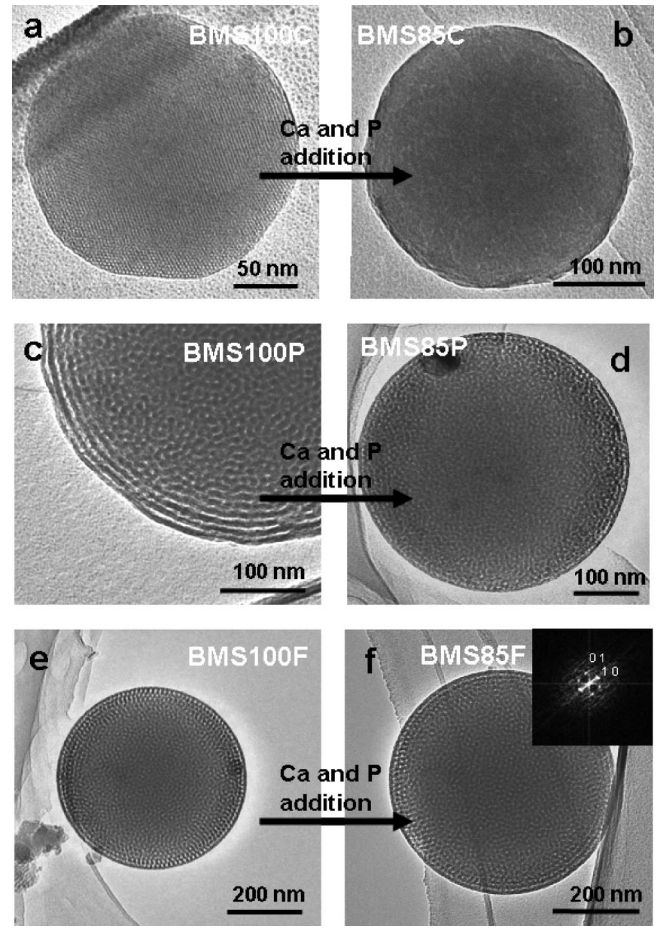

Figure 3. TEM images of BMS100x and BMS85x microspheres synthesized with CTAB, P123, and F127. Magnification 30 000×. Fourier transform pattern for BMS85F is shown, demonstrating the hexagonal mesoporous ordering remaining in this sample.

work. Images a and b in Figure 3 show BMS100C and BMS85C, respectively, i.e., microspheres synthesized with CTAB. Pure SiO_2 microspheres (BMS100C) exhibit highly ordered hexagonal mesoporous structure. On the contrary, BMS85C microspheres show an amorphous mesostructure, as can be seen in Figure 3b, where a whole disordered structure impedes the observation of the contrasts between pores and inorganic walls. Images c and d in Figure 3 shows the TEM images of BMS100P and BMS85P, respectively, i.e. those microspheres synthesized with P123 as surfactant. BMS100P exhibits an ordered lamellar phase at the outer part of the microspheres, which coexists with a wormlike disordered mesoporous structure at the inner part. BMS85P shows an even lower mesoporous ordering, where the lamellar phase at the outer part almost disappears and the wormlike structure dominates the most of the microspheres volume. Finally, images e and f in Figure 3 show the TEM images of BMS100F and BMS85F, respectively, i.e., those microparticles synthesized with F127 as structure-directing agent. Both, pure SiO_2 and 85 SiO_2−5 P_2O_5−10 CaO, synthesized with a highly hydrophilic nonionic surfactant (F127), exhibit a well-ordered mesopore hexagonal arrangement at the outer part (as determined by XRD and FT patterns shown in the inset), which coexists with a low-ordered wormlike mesoporous phase in the inner zone.

Table 1. Textural Properties of the Mesoporous Microspheres Obtained by N_2 Adsorption Porosimetry

sample	pore diameter (nm)	S_{BET}(m^2 g^{-1})	Δ%[a]
BMS100*[b]	4.7	6.5	0
BMS85*[b]	4.7	6.5	
BMS100C	1.8	800	−40
BMS85C	1.1/3.7[c]	484	
BMS100P	5.1	432	−12
BMS85P	3.9	380	
BMS100F	3.5	254	8
BMS85F	3.5	275	

[a] Surface area difference between SiO_2 and $SiO_2-CaO-P_2O_5$ microspheres obtained with the same surfactant. [b] Microspheres obtained without surfactant. [c] BMS85C shows a bimodal pore size distribution.

Textural properties of BMS100x and BMS85x materials are presented in Table 1. For comparison purposes, samples synthesized without any surfactant are included. In that case, the chemical composition of the inorganic pore wall does not affect the textural parameters of the microspheres. The incorporation of any structure directing agent results in an important increase of the S_{BET} values, as a consequence of the mesoporosity formed after the surfactant removal. However, the textural parameters also depend on the microspheres composition (pure SiO_2 or $SiO_2-CaO-P_2O_5$ systems) in combination with the surfactant added. For those mesoporous microspheres derived from CTAB as structure directing agent, a remarkable S_{BET} decrease is observed (around 40% respect to pure SiO_2) when $10CaO-5P_2O_5$ takes part of the composition, as well as a pore diameter modification. With regards to nonionic surfactants, P123-related structures also feature a significant surface reduction and pore size variations $10CaO-5P_2O_5$ is incorporated. This fact is even more evident for samples with higher Ca^{2+} content like BMS75P and BMS58P (see the Supporting Information). On the contrary, pore size variation is negligible and no surface area decrease, but instead a small increase, is observed when BMS100F and BMS85F are compared.

Figure 4 shows the nitrogen adsorption isotherms and pore diameter distributions of BMS100x and BMS85x materials. All isotherms are identified as type IV according to IUPAC classification.[43] However, some differences in the hysteresis loops are appreciated. Sample BMS100C presents an isotherm with almost no hysteresis, characteristic of MCM-41 mesoporous materials,[44] whereas BMS85C exhibits an enlarged hysteresis loop, which can be identified as type H2 defined by a smoothly increasing adsorption branch and a steep desorption branch.[45] Both samples show an important contribution to the volume at the low pressure micropore region. This feature is indicative of a pore diameter enlargement, which allows the nitrogen condensation, as well as an ink-bottle morphology of the pores.[46] A similar phenomenon can be observed in P123 templated materials. Sample

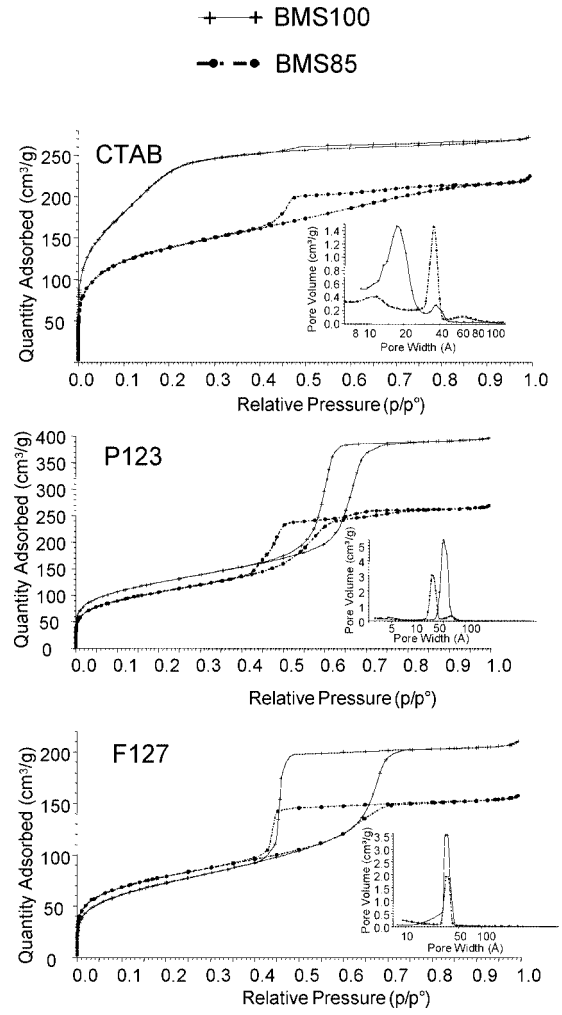

Figure 4. N_2 sorption isotherms and pore size distribution of BMS100x and BMS85x microspheres synthesized with CTAB, P123, and F127.

BMS100P shows a H1 hysteresis loop, representative of pores opened at both sides and narrowing along the pore. However, the isotherm of BMS85P displays a hysteresis loop that seems to be a convolution of two (H1 and H2) loops. In the case of materials synthesized with F127, both BMS100F and BMS85F, a large hysteresis loop of type H2 is found. Although no significant changes are observed in the hysteresis loop morphology, the slightly higher adsorption at the micropore region would explain the higher S_{BET} value in BMS85F.

Figure 5 shows the Ca, P, and Si SBF content as a function of the soaking time for BMS85F. An increase in the Ca content in the SBF can be observed during the first 24 h, reaching values of 150 ppm. Thereafter, the Ca concentration decreases to the original values (around 100 ppm) after 1 week in SBF. The curve observed for the Si concentration shows an increase during the first 24 h reaching values of 55 ppm, showing an asymptotic profile to the end of the test. Finally, the P concentration undergoes a very small increase (about 10 ppm) during the first 3 h of test and thereafter decreases to 16 ppm after 1 week of assay. BMS85C and BMS85P showed almost identical profiles. These release profiles correspond to the sequence of reactions that start with the $Ca^{2+}-H^+$ ionic exchange between the glass

(43) Everett, K. S. W., D. H.; Haul, R. A. W.; Moscou, L.; Pierotti, R. A.; Rouquerol, J.; Siemieniewska, T. *Pure Appl. Chem.* **1985**, *57*, 603.
(44) Schmidt, R.; Hansen, E. W.; Stöcker, M.; Akporiaye, D.; Ellestad, O. H. *J. Am. Chem. Soc.* **1995**, *117*, 4049.
(45) Morishige, K.; Tateishi, N.; Fukuma, S. *J. Phys. Chem. B* **2003**, *107*, 5177.
(46) Van Der Voort, P.; Ravikovitch, P. I.; De Jong, K. P.; Benjelloun, M.; Van Bavel, E.; Janssen, A. H.; Neimark, A. V.; Weckhuysen, B. M.; Vansant, E. F. *J. Phys. Chem. B* **2002**, *106*, 5873.

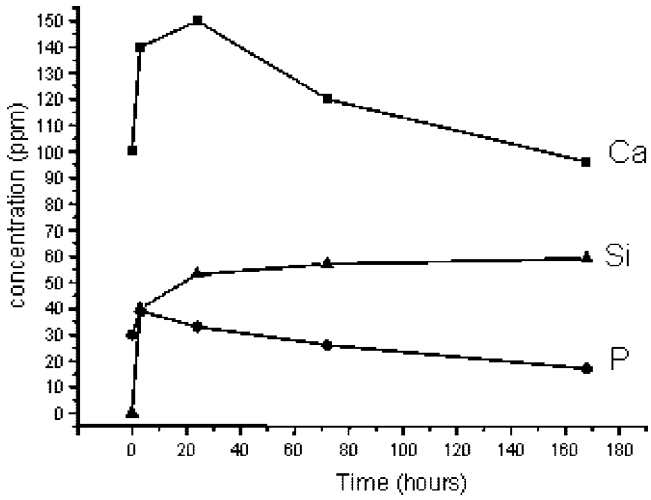

Figure 5. Concentrations of Ca, P, and Si in the SBF as a function of soaking time for sample BMS85F. Samples BMS85P and BMS85C showed almost identical release profiles.

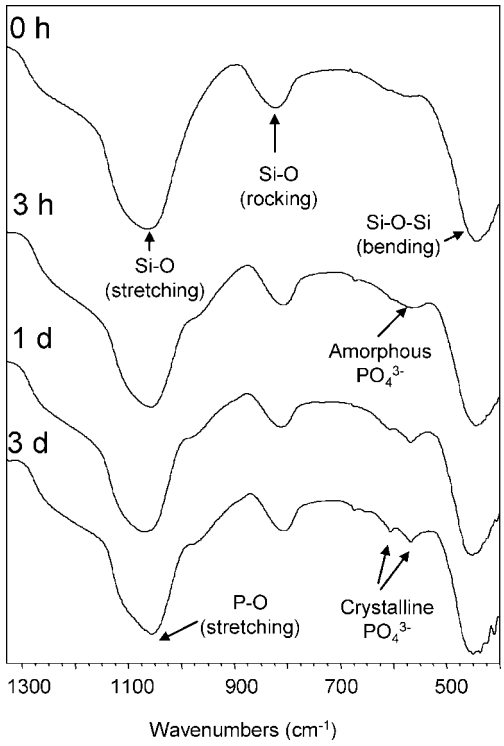

Figure 6. FTIR spectra of BMS85F mesoporous microspheres as a function of soaking time in SBF. Samples BMS85P and BMS85C showed almost identical spectra for the same soaking times.

and the surrounding fluid, and the partial degradation of silica network proposed by Hench.[47] This process leads to the formation of a hydrated silica layer at the surface of the microspheres. Subsequently, Ca and P precipitate to nucleate a new formed calcium phosphate phase. FTIR spectra collected from the surface of BMS85F as a function of soaking time in SBF demonstrate this fact (Figure 6). The spectra of BMS85C and BMS85P undergo the same evolution after immersing in SBF. Before soaking, all the spectra show characteristic absorption bands corresponding to Si−O bonding (1040, 800, 470 cm^{-1}). After 3 h of soaking in SBF, a band at 600 cm^{-1} corresponding to amorphous phosphate can be observed in the spectra of all the samples. After 1 day of soaking, this band begins to split into a doublet at 560 and 600 cm^{-1}, corresponding to phosphate groups in a crystalline environment.

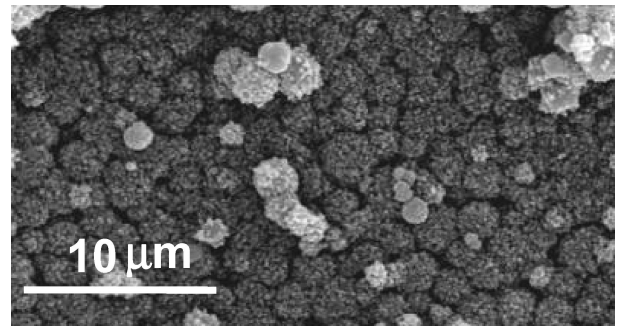

Figure 7. SEM micrographs of BMS85P after soaking in SBF for 3 days.

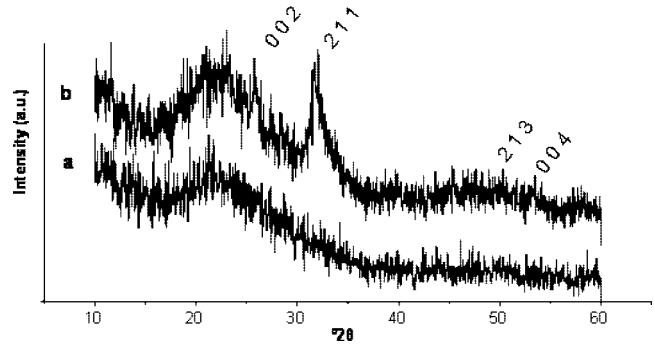

Figure 8. XRD patterns of BMS85C (a) before and (b) after soaking one day in SBF.

As an example, Figure 7 shows SEM micrographs of BMS85P after immersion in SBF for 1 day. It can be observed that microspheres are covered by a new layer of particles, mainly composed by calcium and phosphorus as indicated the EDX analysis (data not shown). Samples BMS85C and BMS85F showed almost identical behaviors when soaked in SBF for the same time.

XRD diffraction patterns of BMS85C (a) before and (b) after soaking in SBF for 1 day are displayed in Figure 8. BMS85C shows only a wide maximum, characteristic of amorphous silica-based glasses. After 1 day of immersion in SBF, diffraction maxima, which can be assigned to the reflections 002, 211, 213, and 004 of an apatite-like phase, can be clearly distinguished. XRD patterns for BMS85P and BMS85F showed similar profiles after 1day of immersion in SBF. For comparison purposes, BMS85* was also soaked in SBF and no bioactive behavior could be observed from FTIR spectra, XRD patterns and/or SEM observations for the same immersion times. On the contrary, porous microspheres with higher Ca^{2+} content (BMS75x and BMS58x) exhibit faster bioactive processes, as could be expected from the common behavior of sol−gel SiO_2−CaO−P_2O_5[48−50] and

(47) Hench, L. L. Andersson O. In *Bioactive Glasses. An Introduction to Bioceramics*; Hench, L. L., Wilson, J., Eds.; Elsevier Science: New York, 1995; p 477.

(48) Pereira, M. M.; Clark, A. E.; Hench, L. L. *J. Biomed. Mater. Res.* **1994**, *28*, 693.

(49) Peltola, T.; Jokinen, M.; Rahiala, H.; Levanen, E.; Rosenholm, J. B.; Kangasniemi, I.; Yli-Urpo, A. *J. Biomed. Mater. Res.* **1999**, *44*, 12.

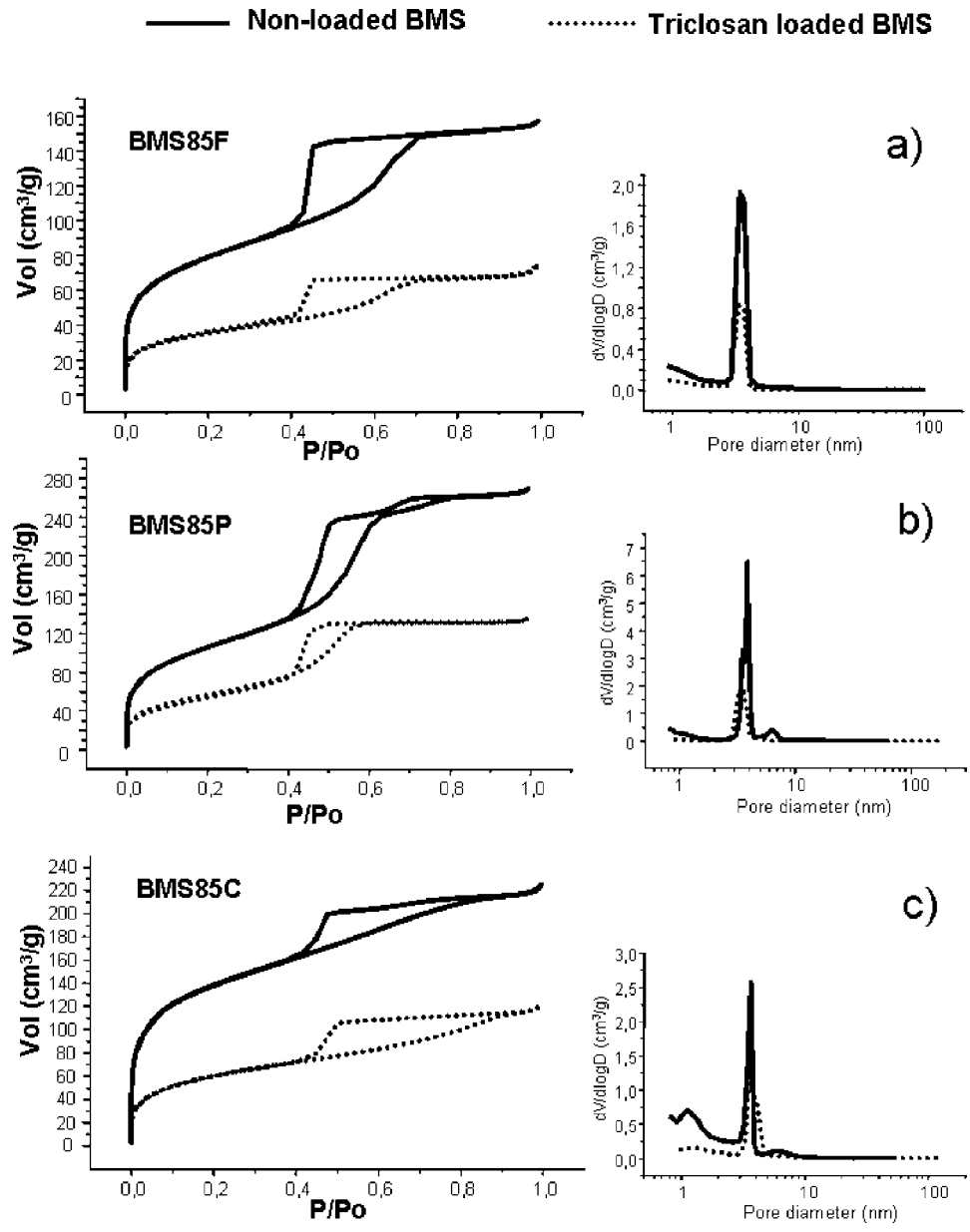

Figure 9. N_2 sorption isotherms and pore size distribution before and after loading with triclosan of (a) BMS85F, (b) BMS85P, and (c) BMS85C.

SiO_2-CaO[51] bioactive glasses (see Figure S3 in the Supporting Information), i.e., the higher the Ca^{2+} content in the glass, the more intense the bioactive behavior, in terms of kinetics and amount of growth of a new apatite-like phase growth on the surface.

To study the drug incorporation into the BMSs, N_2 adsorption porosimetry was also carried out after triclosan loading. Figure 9 shows the adsorption isotherms and pore size distribution for the three different BMS85x samples, before and after loading with triclosan. As a general trend, isotherms display a decrease of the N_2 adsorption capacity after loading with triclosan. This is reflected in a reduction of surface area and pore volume, as a consequence of the pore filling with triclosan (see Table 2). On the contrary, pore diameter is not significantly affected after the drug loading. It must be highlighted that, in the case of BMS85F and BMS85P, the porosity decrease mainly affects the mesopore region. These results indicate that the drug is mainly adsorbed within the accessible mesopores of the material. On the contrary, the porosity reduction for BMS85C mainly affect the micropore region

Table 2. Textural Properties of the BMS85x Microspheres Synthesized with Different Surfactants, before and after Loading with Triclosan

sample	S_{BET} (m^2/g)	pore size (nm)	pore volume/ micropore volume (cm^3/g)
BMS85C	484	1.1/3.7	0.35/0.06
BMS85C-triclosan	219	3.7	0.18/0.01
BMS85P	380	3.9	0.42/0.01
BMS85P-triclosan	198	3.3	0.21/-
BMS85F	275	3.5	0.24/0.02
BMS85F-triclosan	123	3.5	0.11/0.01

(50) Vallet-Regí, M.; Ragel, C. V.; Salinas, A. J. *Eur. J. Inorg. Chem.* **2003**, *6*, 1029.
(51) (a) Martínez, A.; Izquierdo-Barba, I.; Vallet-Regí, M. *Chem. Mater.* **2000**, *12*, 3080. (b) Vallet-Regí, M.; Izquierdo-Barba, I.; Salinas, A. J. *J.Biomed. Mater. Res.* **1999**, *46*, 560. (c) Salinas, A. J.; Martín, A. I.; Vallet-Regí, M. *J. Biomed. Mater. Res* **2002**, *61*, 524.

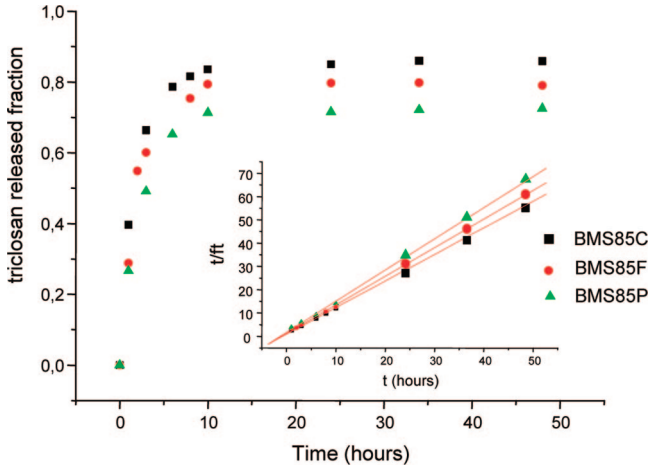

Figure 10. Percentage of triclosan released from loaded BMS85F, BMS85P, and BMS85C as a function of time in an in vitro assay. The inset shows the linearized functions of the three hyperbolic release profiles.

(around 85% of the micropore volume is lost), pointing out that the drug incorporation within the inner mesopores is partially impeded and is mainly adsorbed at the micropores of the outer sphere surface. The low accessibility of the drug to the mesopores of BMS85C would agree with the TEM studies (see Figure 3), where no accessible mesoporosity can be observed for this sample. Besides, mesoporous ordering (in the case of BMS85F) and bioactive behavior were not modified after triclosan adsorption (see Figures S4 and S5 in the Supporting Information).

To study the role of the mesopore structure on the drug release, we evaluated triclosan-loaded BMS85C, BMS85F, and BMS85P spheres as drug delivery systems. These samples were chosen because they have the same chemical composition and bioactive behavior, whereas their mesopore structures are significantly different. TG and CHN elemental analyses determined a triclosan loading of 9.1, 9.7, and 10.7% in weight for BMS85F, BMS85P, and BMS85C, respectively. Figure 10 shows the triclosan release profile for BMS85x samples. The three BMSs exhibit a common behavior based on a first fast release, in which most of the loaded drug is delivered to the medium within 6 h of assay. Afterward, a more controlled pattern is observed until the end of the experiment. This two-step release behavior corresponds to the situation in which triclosan molecules are partly attached to the outer surface of the material, whereas the rest have penetrated the mesoporous network. The release profile can be fitted to a hyperbolic function such as

$$f_t = t/(a + bt)$$

where f_t is the fraction of drug release at time t and a and b are adjustable parameters with phenomenological meanings: $1/b$ is the maximum release and $1/a$ is the initial release rate (slope of the release curve at time = 0). This function can be linearized (see inset in Figure 10) to

$$t/f_t = a + bt$$

and the parameters a and b are extracted by a least-squares fitting of the experimental results, as is plotted in the inset of Figure 10b. The values obtained for the maximum release fraction ($1/b$) and the initial release rate ($1/a$) are shown in Table 3. Although a common release profile is observed for the three kinds of samples, statistically significant differences can be distinguished regarding the calculated kinetic parameters mainly between BMS85C and BMS85P. Sample BMS85F exhibits intermediate values of maximum release fraction and initial release rate values between the other two microspheres.

Table 3. Triclosan Release Kinetic Parameters for Samples BMS85C, BMS85F, and BMS85P

	maximun release fraction	initial release rate (h^{-1})	R
BMS85C	0.88(±0.01)	1.1(±0.2)	0.9999
BMS85F	0.81(±0.01)	0.9(±0.2)	0.9996
BMS85P	0.75(±0.01)	0.6(±0.1)	0.9997

Discussion

Bioceramics intended as matrixes for drug delivery and bone tissue regeneration are required to possess a well-defined particle morphology, with the aim of controlling the drug kinetic release as well as the surface events during the bioactive process. In this sense, nonaggregated bioactive microspheres exhibit much more interesting features compared to bulky irregular particles, often associated into aggregates with noncontrolled sizes. In this frame, EISA synthesis carried out through an aerosol-assisted method demonstrates that it is possible to synthesize mesoporous microspheres with high surface area and pore volume, which present bioactivity. Despite presenting size poly dispersity, spheres synthesized by this technique are not aggregated independently of the surfactant used during the synthesis. This fact confirms the validity of the aerosol-assisted method to produce bioactive mesoporous microspheres.

The incorporation of structure-directing agents to the precursor solutions leads to the formation of mesoporous microspheres. However, the arrangement and ordering degree strongly depends on two factors, i.e. chemical composition of the inorganic phase and type of surfactant (ionic or nonionic). Actually, pure SiO_2 microspheres exhibit some kind of mesopore ordering independently of the surfactant used. However, the addition of cationic surfactants such as CTAB, seems to form hexagonal arrangements with higher ordering degree than those resulting from the addition of nonionic triblock copolymers (P123 and F127), as could be evidenced by TEM observations.

Though pure SiO_2 microspheres evidence mesoporous arrangement that depends on the surfactant added, as well as high surface area and porosity values, only $SiO_2-CaO-P_2O_5$ mesoporous microspheres develop an apatite like phase in contact with SBF, evidencing that the presence of CaO (P_2O_5 only modifies the kinetic growth of the new formed apatite phase[51]) and high textural values (surface area and porosity) are mandatory for the expression of bioactive behavior. According to the collective examination of FTIR spectra, XRD and SEM observations after bioactivity assays, a new layer of apatite crystallizes on the surface of the mesoporous materials after 1 day of immersion in SBF, whereas no changes could be observed in materials obtained without surfactant addition. This fact confirms the high dependency of the bioactive process on the surface

properties of the material. Nevertheless, despite BMS85C, BMS85P, and BMS85F having very different surface area parameters, they present an almost identical bioactive performance. This fact suggests that for the same calcium content, there is a surface value threshold for these systems to be bioactive.

Especially interesting are the mesostructural and textural changes undergone by the microspheres after CaO addition. As mentioned above, the CaO incorporation leads to defective structures and decreases the ordering degree as a function of the surfactant used. Consequently, the changes introduced by Ca^{2+} cations will be different depending on the ionic or nonionic surfactant composition. The formation of a silica−surfactant hybrid interface is mandatory for a well-defined mesophase formation. From the point of view of the thermodynamic aspect, Huo et al.[52] postulated that the most relevant aspects in the formation of the hybrid mesophase (ΔG_{ms}) are

$$\Delta G_{ms} = \Delta G_{inter} + \Delta G_{inorg} + \Delta G_{org} + \Delta G_{sol}$$

ΔG_{inter} is related to the formation of a well-defined hybrid interface, whereas ΔG_{org} and ΔG_{inorg} define the thermodynamic of surfactant micelles formation and positioning of the inorganic component, respectively. ΔG_{sol} involves the influence of the solvent respect to both surfactant and inorganic species. The condensation of the silica species should not disrupt the organization of a well-defined hybrid interphase. Consequently, $|\Delta G_{inter}|$ must be higher than $|\Delta G_{inorg}|$ for achieving a well-defined mesostructure. From the point of view of kinetic aspects, it is important that the kinetic constants of the different processes fulfill the following condition

$$k_{inter} > k_{org} > k_{inorg}$$

In these conditions, the formation of the mesostructure is controlled by the hybrid interface, leading to ordered phases through self-assembly processes.[53] Because the silica polymerization is very slow at the pH used in this work (pH < 2,) this condition is fulfilled in the case of pure SiO_2 microspheres, and ordered mesoporous materials are obtained for the three surfactants used. On the contrary, the displacement of the positively charged silica species by the Ca^{2+} cations modifies the needed thermodynamics and kinetic conditions, especially in those cases where the hybrid interface is strongly dependent on ionic interactions. For instance, synthesis of mesoporous materials using CTAB as template in a strongly acid medium involves an interaction type $SiOH^+-A^--S^+$, where charged surfactant interacts with silanol groups of the new-forming silica network by means of a bonding anion, (bromide and nitrate in this case). When calcium cations are added to the medium, they interact with these anions displacing the $SiOH^+$ species and impeding a correct surfactant−anion−silica interaction, and the appearance of a defective mesostructure takes place in BMS85C.

In the case of nonionic surfactants, mesophase formation is mediated by an interaction between silanol groups and the hydrophilic parts of the surfactants together with ionic interactions of the type $(S^0H^+)(X^-I^+)$ that contribute to the formation of the hybrid interface. Our TEM studies indicate that Ca^{2+} cations do not affect the hexagonal structure in BMS85F. In addition, the structure of BMS85P closely resembles to that of BMS100P. In these situations, the Ca^{2+} cations influence is weaker because of the nonionic character of the surfactant.

The ability of BMS materials to be used as drug carriers has been tested through a release essay employing triclosan as model drug. This organic molecule is a antimicrobial agent for the treatment of supragingival plaque. Periodontal diseases are caused by bacterial infection,[54] and a prolonged release of therapeutic agent beyond application should be desirable. Whereas the release profiles are similar for the three studied samples, the kinetic parameters depend on the porous structure. BMS85C shows the fastest initial release rate and the highest value for the maximum released fraction. These two values would indicate that most of triclosan would be adsorbed on the microporous external surface of the BMS85C microspheres. The high micropore content (see Figure 4) and the absence of mesopores accessible at the microspheres surface (see TEM image in Figure 3b) would lead to the accumulation of triclosan at the outer surface of the microsphere location. In addition, the significant microporosity decrease observed after triclosan loading clearly indicates that these microspheres mostly retain the drug at the outer surface, with low adsorption onto the inner mesopores.

On the contrary, BMS85P exhibits the slower initial release rate and the lower maximum released fraction, indicating that triclosan is better adsorbed within the inner location of the microspheres. This would agree with the accessible mesoporosity to the spheres surface as observed by TEM. BMS85F exhibits intermediate initial release rate and maximum released fraction values between BMS85C and BMS85P. Although BMS85F kinetic parameters are not significantly different than those of BMS85C and BMS85P, this intermediate situation could be understood in terms of deeper drug adsorption compared with BMS85C (because of the accessible mesoporosity), but a faster drug release than BMS85P because of the lower tortuousness of the ordered hexagonal matrix (BMS85F) compared with the wormlike porous structure exhibited by BMS85P. However, these differences in release rate do not seem to be of significant importance (from a quantitative point of view), when envisioning the potential clinical applications, although they contribute to characterize the drug location in the different microspheres. Other synthesis strategies, such as surface funtionalisation, would contribute to deeply modifying the release profiles.

Anyway, the release profile shown by this material could be suitable for helping plaque removal with a first high triclosan dose, followed by a sustained release. This effect confers an added value for BMS materials as periodontal regenerative surgery and infection prophylaxis.

(52) Huo, Q.; Margolese, D. I.; Ciesla, U.; Demuth, D. K.; Feng, P.; Gier, T. E.; Sieger, P.; Fioruzi, A.; Chmelka, B. F.; Schüth, F.; Stucky, G. D. *Chem. Mater.* **1994**, *6*, 1176.

(53) Soler-Illia, G. J. A. A.; Sanchez, C.; Lebeau, B.; Patarin, J. *Chem. Rev.* **2002**, *102*, 4093.

(54) Piñón-Segundo, E.; Ganem-Quintanar, A.; Alonso-Pérez, V.; Quintanar-Guerrero, D. *Int. J. Pharm.* **2005**, *294*, 217.

Conclusions

Bioactive microspheres with a mesoporous ordering have been synthesized via aerosol-assisted technique. Three surfactants have been tested as structure-directing agents: a cationic surfactant, CTAB, and two nonionic triblock copolymers, F127 and P123, with different lengths of the hydrophilic chains.

Multicomponent $SiO_2-CaO-P_2O_5$ inorganic pore walls lead to materials that present bioactive behavior, regardless of surfactant type. Those microspheres templated by CTAB present a higher deterioration of the mesopores arrangement. In the case of nonionic surfactants, F127 shows a less remarkable alteration of structural and textural properties. Bioactive microspheres synthesized with this surfactant have proved the ability to act as a drug delivery system.

The combination of bioactive behavior and drug release properties suggests the suitability of these materials for periodontal regenerative surgery and infection profilaxis.

Acknowledgment. The financial supports of CICYT Spain, through Research Project MAT2005-01486, CAMS-0505/MAT/000324, VR: Sweden, and JST Japan (O.T.) are acknowleged. We also thank F. Conde (CAI X-ray Diffraction, Universidad Complutense), Electron Microscopy Center, and CAI Microanálisis, Universidad Complutense, for their valuable technical assistance.

Supporting Information Available: Additional table, XRD patterns, FTIR spectra, and bioactivity assay afer triclosan loading (PDF). This material is available free of charge via the Internet at http://pubs.acs.org.

CM801649Z